Journal of the Korean Physical Society
https://doi.org/10.1007/s40042-023-00811-z

Online ISSN 1976-8524
Print ISSN 0374-4884

ORIGINAL PAPER - CROSS-DISCIPLINARY PHYSICS AND RELATED AREAS OF SCIENCE AND TECHNOLOGY

Polymeric gate insulators to induce synaptic photoresponse of organic transistors

Gyu-Min Ko[1] · Yu Gyeong Kang[2] · Ui-Chan Jeong[1] · Tae-Woo Lee[2,3] · Hea-Lim Park[1]

Received: 21 March 2023 / Revised: 10 April 2023 / Accepted: 10 April 2023

Abstract
Photonic synapses have attracted increasing interest owing to their ultrafast signal transmission, high bandwidth, and low energy consumption. Dielectrics in organic photonic synaptic transistors (OPSTs) affect the photoinduced charge accumulated at the interface between the dielectrics and organic semiconductor (OSC) layer, modulating a synapse-like behavior. Herein, to investigate the effect of the interfacial properties of polymeric gate insulators on photosensitive synaptic characteristics, two types of polymers, i.e., poly(4-vinylphenol) and poly(styrene), were used as gate dielectrics of OPSTs. We discovered that the functional groups of the polymeric gate dielectrics that induce charge trapping primarily contribute to the synaptic properties of the OPSTs. This result was obtained by analyzing the morphological and physicochemical properties, including surface roughness, surface energy of the insulators, and grain size of the OSC layer on the dielectric layers. Further, the poly(4-vinylphenol)-based OPST with strong interfacial charge-trapping effect showed various synaptic characteristics, such as excitatory postsynaptic currents, paired-pulse facilitation, spike duration-dependent plasticity, spike number-dependent plasticity, and spike rate-dependent plasticity, according to the adjustment of various ultraviolet light information (i.e., exposure duration, number, and rate). In contrast, the poly(styrene)-based OPST did not show synaptic photoresponse. Furthermore, based on the potentiation/depression characteristics of the device, a recognition accuracy of 88% was achieved using handwritten digit recognition designed using datasets from the Modified National Institute of Standards and Technology. Therefore, this study reveals the understanding of the relation between the dielectric/OSC layer and photosensitive synaptic characteristics from the charge-trapping effect. It also provides a strategy for optimizing the photoresponsive synaptic characteristics of OPSTs.

Keywords Artificial synapse · Organic photonic synaptic transistor · Interfacial charge-trapping effect · Functional group · Polymer gate insulator

1 Introduction

Conventional computers based on the von Neumann architecture cannot efficiently handle unstructured data because of memory and processing unit separation. Furthermore, physically separating memory and the processing unit requires continuous data transmission between them, causing a von Neumann bottleneck. This also leads to large energy consumption and degrades computing performance [1, 2]. Bioinspired neuromorphic electronics mimicking the human brain have emerged as a new computing model to resolve the limitations of the von Neumann architecture. In biological neural networks, synapses are the fundamental units of signal transmission, data processing, and memory. Moreover, synaptic plasticity supports complex perception and cognitive intelligence.

✉ Tae-Woo Lee
twlees@snu.ac.kr

✉ Hea-Lim Park
parkhl21@seoultech.ac.kr

[1] Department of Materials Science and Engineering, Seoul National University of Science and Technology, Seoul 01811, Republic of Korea

[2] Department of Materials Science and Engineering, Seoul National University, Seoul 08826, Republic of Korea

[3] School of Chemical and Biological Engineering, Institute of Engineering Research, Research Institute of Advanced Materials, Soft Foundry, Seoul National University, 1 Gwanak-Ro, Gwanak-Gu, Seoul 08826, Republic of Korea

Published online: 21 April 2023

Therefore, realizing synaptic properties is essential for brain-like computing systems with highly parallel and flexible adaptive capabilities [3–16].

In various types of recently reported synaptic devices, organic photonic synapses that exhibit synaptic characteristics according to light stimulation are attracting attention owing to their high bandwidth, low power consumption, ultrafast signal transmission [17–20], and tunable photoelectric properties through molecular design [21–23]. Notably, understanding the relation between a dielectric layer and an organic semiconductor (OSC) is important, because the transport of photoinduced carriers mainly occurs in several monolayers of the semiconductor layer. This primarily occurs near the interface with the gate insulator, considerably influencing the synaptic characteristics. Many photonic synapses have adopted charge-trapping mechanisms at dielectric/OSC interfaces to demonstrate synaptic properties. This means that various synaptic characteristics are caused by trapping photoinduced charges at the interfaces. However, the interfacial properties of polymer insulators associated with charge-trapping mechanisms and resultant synaptic characteristics have not been sufficiently studied.

In this study, the dependence of the photosensitive synaptic behavior of organic photonic synaptic transistors (OPSTs) on morphological and physicochemical properties at the dielectric/OSC interface was investigated. Two types of polymer dielectric materials, i.e., poly(styrene) (PS) and poly(4-vinylphenol) (PVP), were used. Although these two polymer insulators are structurally similar, PS has no specific functional group, while PVP has a hydroxyl group. Based on the OPSTs with two types of polymeric insulators, interfacial properties, including the surface roughness, surface energy, and grain size of the OSC layer on each dielectric layer, were measured. Additionally, by adjusting ultraviolet (UV) light-stimulation parameters, such as light-exposure duration, number, and frequency, several synaptic characteristics, such as excitatory postsynaptic current (EPSC), paired-pulse facilitation (PPF), spike number-dependent plasticity (SNDP), spike duration-dependent plasticity (SDDP), and spike rate-dependent plasticity (SRDP), were successfully emulated only in the PVP-based OPST. Furthermore, a recognition accuracy of 88% was achieved in numerical simulations based on Modified National Institute of Standards and Technology (MNIST) datasets. Therefore, this study provides a simple and effective strategy for optimizing the high-photosensitive performance of OPSTs for future optoelectronic and neuromorphic devices.

2 Experimental details

First, we fabricated a bottom-gate top-contact OPST on the Si/SiO_2 substrate. Then, the Si/SiO_2 substrate containing a thermally grown, 300 nm-thick SiO_2 layer was cleaned via sonication in acetone and isopropanol (IPA) twice for 10 min, respectively. After sonication, the substrates in the IPA solvent were annealed at 220 °C. For preparing the gate insulator, PS (M_w = 280,000 g/mol; Sigma-Aldrich Korea) was dissolved in toluene at a concentration of 2 wt.%. PVP (M_w = 25,000 g/mol; Sigma-Aldrich Korea) mixed with poly(melamine-*co*-formaldehyde) (crosslinking agent; Sigma-Aldrich Korea) (100 wt.% of PVP) was then dissolved in propylene glycol methyl ether acetate at 2 wt.%. Subsequently, PVP solutions were filtered using a 0.45-μm syringe filter, and PS and PVP solutions were spin coated at 3000 rpm for 30 s, affording a 50-nm thickness. Thereafter, the PS film was annealed at 110 °C for 1 h and PVP was annealed at 110 °C for 10 min and then at 200 °C for 30 min for crosslinking. Furthermore, a 55 nm thickness of pentacene was thermally evaporated on the gate insulator at 0.5 Å/s to form an OSC layer. Subsequently, a 50 nm-thick Au layer was thermally evaporated at a rate of 1.0 Å/s to form the source and drain electrodes with 100- and 1500-μm channel length and width, respectively.

Atomic force microscopy (AFM) (XE-150, PSIA) was used to analyze the morphology of each dielectric layer and pentacene films on the polymeric layers. The electrical characteristics of the device were measured using a semiconductor device analyzer (B1500A, Keysight) under ambient conditions. Finally, synaptic properties (PPF, SDDP, SNDP, SRDP, and potentiation and depression) were measured using a UV light-emitting diode with a 365-nm peak wavelength (light intensity of 9.07 mW/cm^2) under light stimulation. Light intensity was measured by using photometer (ILT 1400-A, International Light Technologies).

3 Results and discussion

A schematic of a biological synapse connecting two adjacent neurons is shown in Fig. 1a. Biological synapses are based on electrochemical interactions, in which neurotransmitters triggered via the action potentials of presynaptic neurons induce synaptic plasticity. In OPSTs, a light spike is regarded as an input signal and the source–drain current serves as an output signal. When the applied light–stimulus parameter is adjusted, the amount of photoinduced electrons accumulated at the interface changes. This changes the current level, which is considered as the postsynaptic response. The device configuration of OPSTs imitating a synapse is shown in Fig. 1b. Pentacene, which is widely used in organic electronic devices owing to its excellent carrier mobility, was used for preparing the semiconducting layer of our photonic synapse. In addition, two polymer gate insulators were used to investigate the effect of the interfacial properties of the dielectric layers on device performance. Results show that the dielectrics used

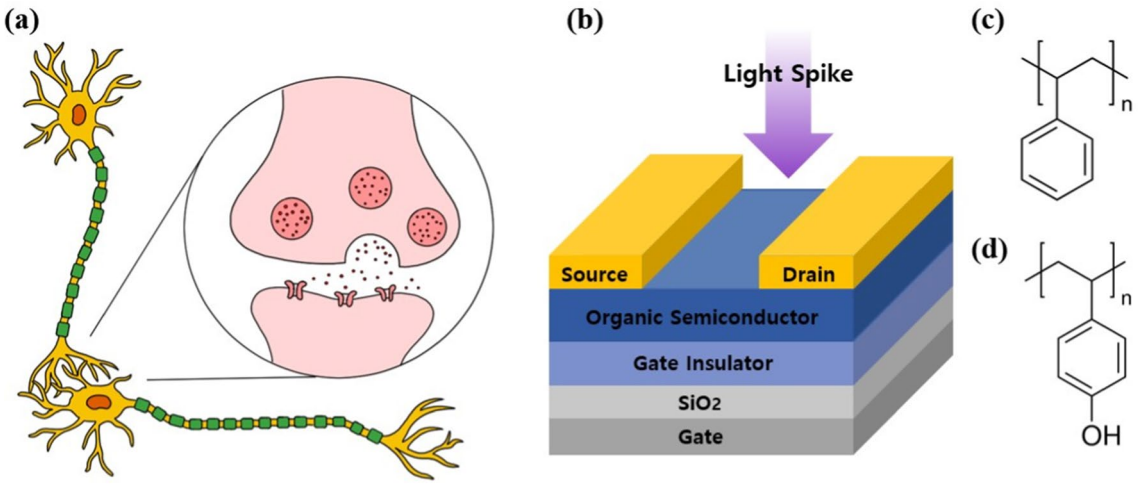

Fig. 1 Schematic of **a** neuron and synapse and **b** organic photonic synaptic transistor configuration. Chemical structure of **c** PS and **d** PVP

in OPSTs have similar molecular structures; PS has no specific functional group, while PVP has hydroxyl groups (Fig. 1c, d). Details of the device fabrication process are described in the experimental section.

The large surface roughness of gate insulators affords a small grain size and a high grain boundary density of OSC layers, causing increased charge trapping [24]. The morphological properties of the two polymer insulators were analyzed using the AFM images to investigate the interfacial characteristics of different polymer insulators. The AFM images of PS and PVP layers are shown in Fig. 2a and b, respectively. The morphological profiles of PS and PVP along the dash lines marked in Fig. 2a and b, respectively, are shown in Fig. 2c. The root-mean-square roughness values of the PS and PVP layers are 0.29 and 0.23 nm, respectively. A previous study reported that this range of root-mean-square roughness had little effect on grain size; thus, the effect of surface roughness on charge trapping is expected to be similar in both OPSTs [25]. The contact angles of water droplets on the PS and PVP layers are presented in Fig. 2d. Compared with the contact angle of PS (81°), PVP showed a lower contact angle (65°), indicating higher surface energy. A previous study showed that PVP exhibits higher surface free energy and lower contact angle than PS because of the influence of the polarity of the hydroxyl group [26]. The AFM images of 10 nm-thick pentacene films on the PS and PVP layers are shown in Fig. 2e and f, respectively. These films were investigated because a few OSC monolayers deposited on the gate insulator are expected to directly contribute to photogenerated charge transport [27]. The average grain size of pentacene on the PS and PVP layers was similar [28]. This means that the charge-trapping density in the grain boundary, which is closely related to the synaptic behavior, can be similar.

The transfer curves of OPSTs using PS (Fig. 3a) and PVP (Fig. 3b) as gate dielectrics were investigated before and under UV light irradiation to understand the influence of the dielectric/OSC interface characteristics on photoresponse. Electron–hole pairs (EHPs) are generated through UV light irradiation with higher photon energies than the energy band gap of the pentacene film. PVP showed a larger threshold voltage shift toward the positive direction than PS (Fig. 3a, b). Additionally, because the surface roughness of the PS and PVP layers and the grain sizes of the pentacene layers on them were similar, the distinct photoresponse is mainly attributed to the functional groups of the dielectric molecules. The polarity of polymeric insulators contributes to the wettability. The hydrophilicity of PVP increases the amount of absorbed water, causing electron trapping at the OSC/gate insulator interface [26, 29]. Photoinduced electrons trapped at the dielectric/OSC interface by hydroxyl groups act as an additional negative gate bias, increasing the drain current under light illumination [30–32]. The dynamic photoresponsive behavior of each OPST was investigated. The drain current was measured under a UV exposure of 10 s at an interval of 10 s (Fig. 3c, d). The drain current of PS and PVP OPSTs immediately increased when UV-light illumination began because photoinduced EHPs were generated. During light exposure (shaded area), the photocurrent of PVP gradually increased over time as the negative charges strongly trapped at the interface generated additional gate voltage, unlike PS, where the current level remained constant. As the light was turned off, PS recovered to its initial state while in the case of PVP, the device slowly returned to its initial state. The PS gate insulator could not hold the photoinduced charge owing to the absence of a specific functional group, causing it to return to the initial current when the external stimulus disappeared. Meanwhile, PVP

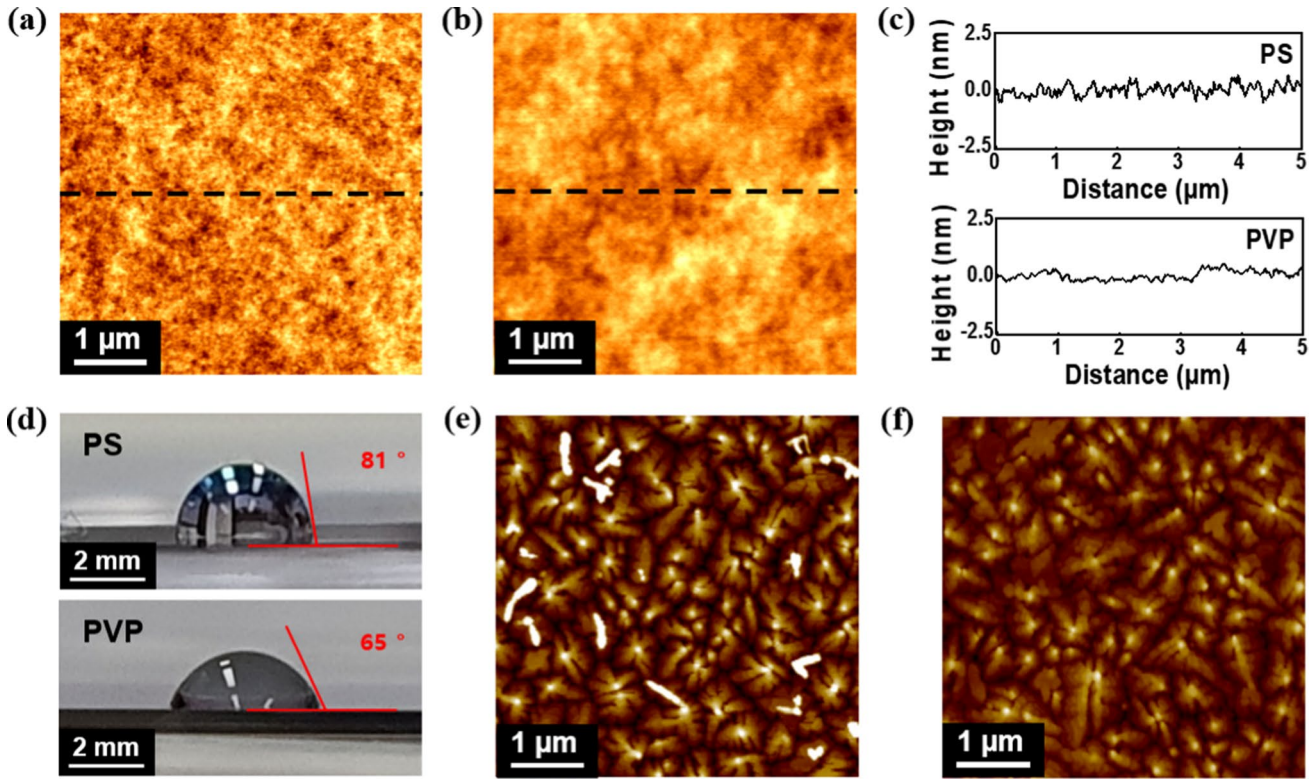

Fig. 2 AFM images of **a** PS and **b** PVP layers. **c** Morphological profiles showing surface roughness along the dashed line of **a** PS (top) and **b** PVP (bottom) layers. **d** Water contact angles on PS (top) and PVP (bottom). AFM images of 10 nm–thick pentacene layers on **e** PS and **f** PVP

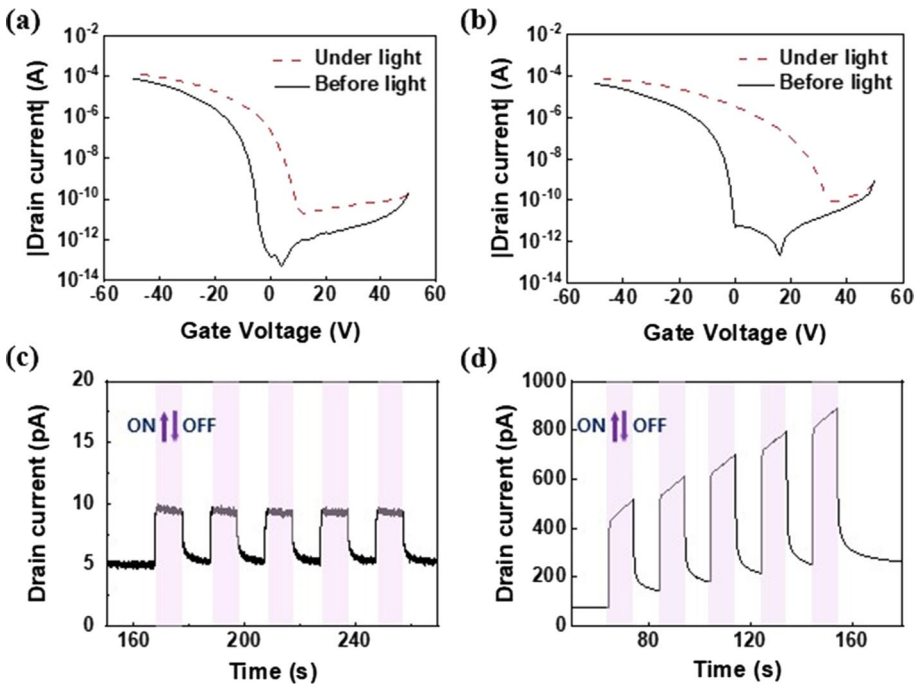

Fig. 3 Transfer curve of OPSTs with **a** PS and **b** PVP gate insulator before and under light irradiation. Current changes of OPSTs with **c** PS and **d** PVP at $V_G = 0$ V and $V_D = -5$ V; the light was repeatedly irradiated as a cycle of 10-s exposure and 10-s turning off

exhibited a delay time until the drain current value returned to the initial state, because the hydroxyl group acted as an electron-trapping site, prohibiting EHP recombination. Thus, the current level gradually increased during UV exposure, implying that hydroxyl groups can provide synaptic properties to the device.

As a form of typical short-term plasticity (STP), PPF can be emulated through continuous charge capturing in a polymer insulator interface, triggered by multiple light spikes. EPSCs triggered by consecutive UV-light spikes at various time intervals are demonstrated in Fig. 4a–c. The EPSC triggered by the second light spike was larger than that triggered by the first spike, which is similar to the PPF behavior of biological synapses. Therefore, the PPF index was defined as A_2/A_1, where A_1 and A_2 are the amplitudes of the first and second EPSC, respectively. The experimental PPF indexes extracted from an OPST with the PVP dielectric layer as a function of optical pulse interval ranging from 20 to 2000 ms are shown in Fig. 4d. The PPF index increased with decreasing time interval. When consecutive light spikes were applied close to the first light spike, photoinduced electrons did not have enough time to return to their initial state. Therefore, the EPSC value obtained after the second spike is larger than that obtained after the first spike.

Synaptic plasticity in the human brain can be divided into two types according to the retention time: STP and long-term plasticity (LTP) [33, 34]. STP can be converted to LTP when repeated stimulation is applied, which is analogous to the learning process of the biological brain. As the light duration increased from 20 to 2000 ms, the EPSC level increased from 99.1 to 176.5 pA (Fig. 5a). These results show that spike duration can modulate the synaptic weight of the OPST. Various numbers of light stimuli were applied on the synaptic transistor to achieve the transition from STP to LTP (Fig. 5b). The peak current gradually increased with the increasing number of light spikes, demonstrating the SNDP characteristics. The SNDP index is defined as A_n/A_1, where A_n is the last peak and A_1 is the first peak (Fig. 5c). The SNDP index (A_n/A_1 values) increased from 1.403 to 3.267 as the spike number increased from 10 to 50. The change in the drain current level triggered by light pulses of frequencies ranging from 0.5 to 10 Hz is shown in Fig. 5d. Five consecutive UV pulses were applied (Fig. 5e) to induce these changes. An SRDP index (A_5/A_1) indicates the ratio of drain current induced by the fifth and the first UV pulses. The SRDP index increased from 1.165 to 1.240 as the frequency increased from 0.5 to 10 Hz. Therefore, the conductivity change caused by a weak input signal lasts for a short time, which corresponds to STP. Notably, the transition from STP to LTP was successful with the increased duration, number, and rate of stimuli.

As shown in Fig. 6a, 30 potentiations were performed under light illumination for a duration of 5.25 s and an interval of 52.5 s. Further, 30 depression levels were realized at $V_D = -35$ V for 32 s and $V_D = -5$ V for 160.5-s intervals. Our synaptic device exhibited a linear potentiation/depression curve under these conditions. Numerical simulations were performed to analyze the potential of the learning ability of the OPST based on potentiation/depression characteristics, creating an intelligent system. A handwritten digit recognition system was simulated through a neural network designed based on the MNIST datasets. This neural network was constructed with three layers connected through synapses. The artificial neural network for the '2' input pattern recognition process and the network, which comprises input (784 neurons), processing (32 neurons), and output layers (10 neurons), are shown in Fig. 6b. Under UV-light illumination, the synaptic device achieved a recognition accuracy of 88%, which is close to that achieved

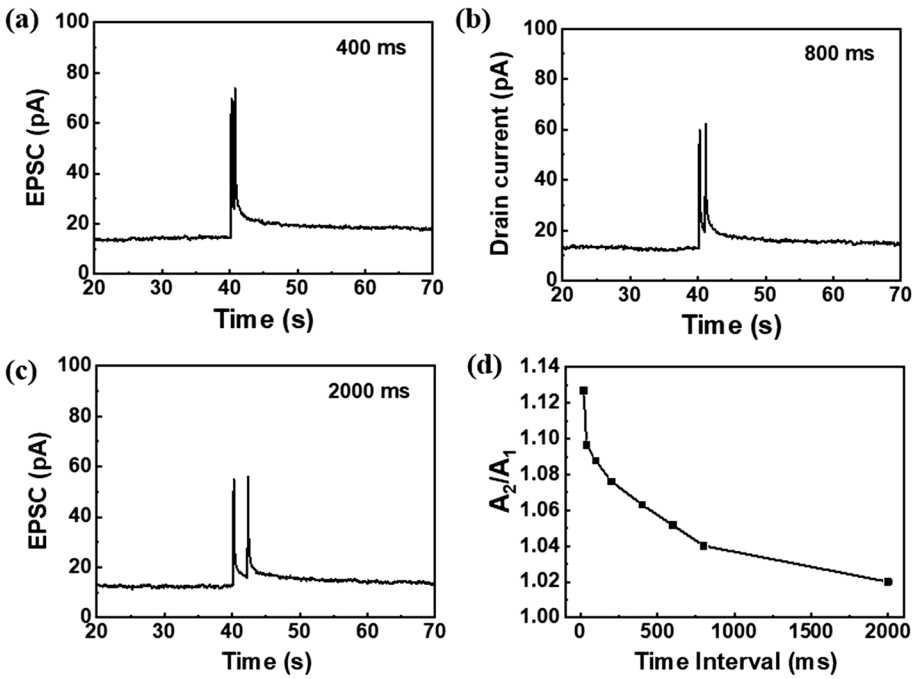

Fig. 4 PPF with time intervals of **a** 0.4, **b** 0.8, and **c** 2 s at $V_G = 0$ V and $V_D = -5$ V. **d** PPF index with various time intervals (20–2000 ms)

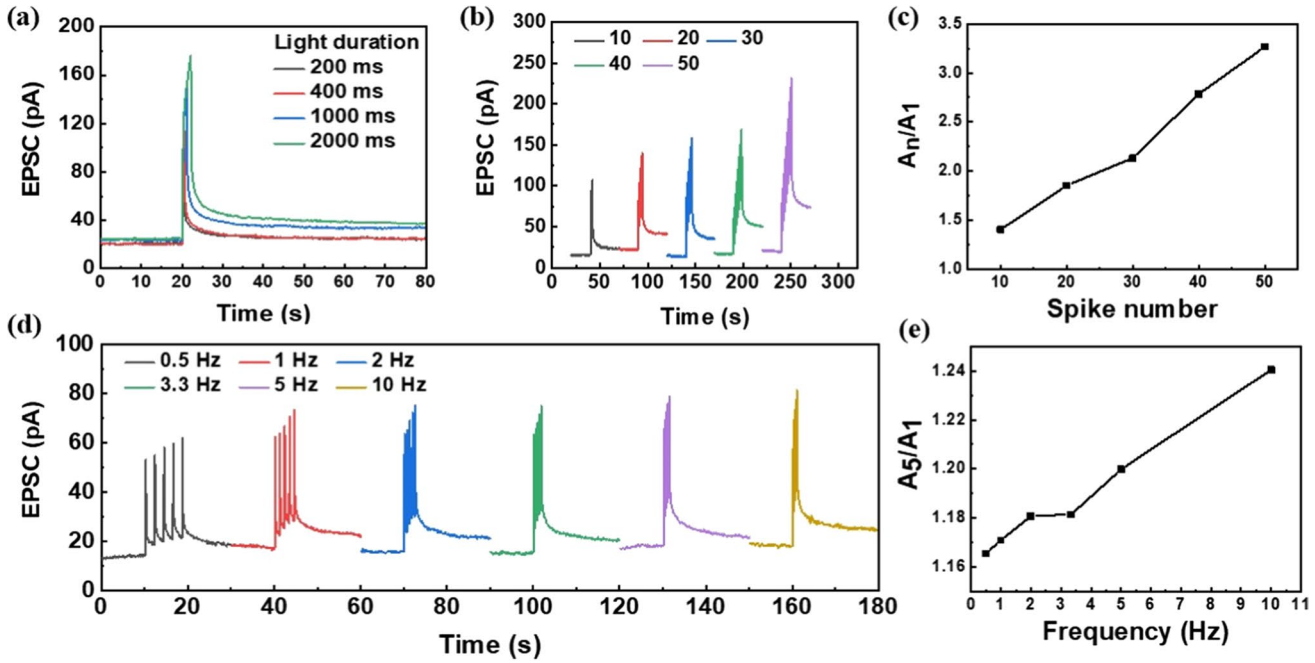

Fig. 5 Synaptic characteristics of OPST under UV exposure. **a** SDDP with a light-irradiation duration of 20–2000 ms at $V_G = 0$ V and $V_D = -5$ V. **b** SNDP with various spike numbers (10–50) at $V_G = 0$ V and $V_D = -5$ V. **c** SNDP index with spike numbers 10 − 50. **d** SRDP with a frequency of 0.5–10 Hz at $V_G = 0$ V and $V_D = -5$ V. **e** SRDP index with various frequencies

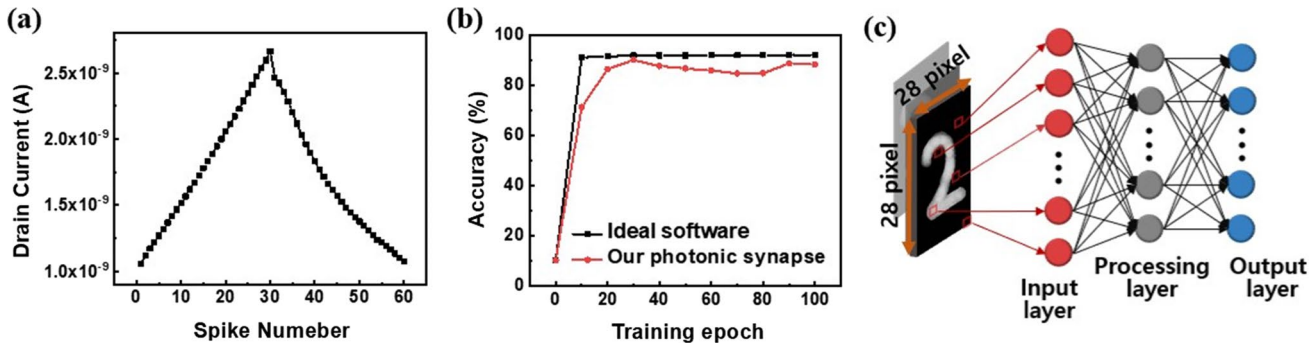

Fig. 6 **a** Potentiation and depression characteristics. Thirty potentiations with a 5.25-s light-irradiation duration and a 52.5-s interval; 30 depressions with $V_D = -35$ V for 32 s and 160.5 s interval at $V_D = -5$ V. **b** Handwritten digit recognition simulation accuracy for ideal software and this work. **c** A neural network to identify handwritten digit images

using an ideal software system. The recognition accuracy can be increased by improving linearity and symmetry of synaptic weight updates in potentiation and depression curves. Higher linearity and symmetry can be achieved by increasing the intensity of the UV light spike applied to the OPST or optimizing the applied voltage condition [35–37].

4 Conclusions

Herein, the influence of interfacial characteristics at the polymeric gate dielectric/OSC interface on the photosensitive synaptic properties of the OPST was investigated.

The analysis of the morphological and physicochemical properties of dielectric/OSC interface and dynamic photoresponse of the OPSTs showed that the hydroxyl group of PVP is mainly responsible for the photonic synaptic characteristics. More specifically, unlike PS (with no specific functional group), the hydroxyl groups of PVP act as photoinduced trapping sites. Based on the functional group, photoinduced electrons trapped at the dielectric/semiconductor interface cannot immediately return to their initial state, providing a synapse-like behavior to the OPSTs. Furthermore, tuning the light-stimulation parameters, such as exposure duration, number, frequency, and the interval between two consecutive light exposures, can modulate synaptic weights. Therefore, synaptic properties, such as EPSC, PPF, SDDP, SNDP, SRDP, and the transition of STP to LTP, were successfully implemented. Moreover, based on the potentiation/depression characteristics of the device, a high recognition accuracy of 88% was achieved in handwritten digit recognition designed using MNIST datasets. By analyzing the surface properties of the OPSTs fabricated with different dielectric layers, we found that the photosensitive synaptic characteristics of the OPST were considerably affected by the functional groups of polymer dielectrics. Therefore, this study provides a simple and effective strategy for optimizing the photosensitive performance of OPSTs for future optoelectric and neuromorphic devices.

Acknowledgements This study was supported by the Research Program funded by SeoulTech (Seoul National University of Science and Technology).

Declarations

Conflict of interest The authors declare no competing financial interest.

References

1. P.A. Merolla, J.V. Arthur, R. Alvarez-Icaza, A.S. Cassidy, J. Sawada, F. Akopyan et al., A million spiking-neuron integrated circuit with a scalable communication network and interface. Science **345**, 668–673 (2014). https://doi.org/10.1126/science.1254642
2. R.F. Service, The brain chip. Science **345**, 614–616 (2014). https://doi.org/10.1126/science.345.6197.614
3. K.N. Kim, M.J. Sung, H.L. Park, T.W. Lee, Organic synaptic transistors for bio-hybrid neuromorphic electronics. Adv. Electron. Mater. **8**, 2100935 (2022). https://doi.org/10.1002/aelm.202100935
4. J.S. Ro, H.M. An, H.L. Park, Electrolyte-gated synaptic transistors for brain-inspired computing. Jpn. J. Appl. Phys. **62**, SE0801 (2023). https://doi.org/10.35848/1347-4065/acaca4
5. M.W. Park, D.Y. Kim, U. An, J. Jang, J.H. Bae, I.M. Kang, S.H. Lee, Organizing reliable polymer electrode lines in flexible neural networks via coffee ring-free micromolding in capillaries. ACS Appl. Mater. Interfaces **14**, 46819–46826 (2022). https://doi.org/10.1021/acsami.2c13780
6. H.L. Park, M.H. Kim, H. Kim, S.H. Lee, Self-selective organic memristor by engineered conductive nanofilament diffusion for realization of practical neuromorphic system. Adv. Electron. Mater. **7**, 2100299 (2021)
7. H.L. Park, T.W. Lee, Organic and perovskite memristors for neuromorphic computing. Org. Electron. **98**, 106 (2021). https://doi.org/10.1016/j.orgel.2021.106301
8. M.H. Kim, H.L. Park, M.H. Kim, J. Jang, J.H. Bae, I.M. Kang, S.H. Lee, Fluoropolymer-based organic memristor with multifunctionality for flexible neural network system. NPJ Flex. Electron. **5**, 34 (2021). https://doi.org/10.1038/s41528-021-00132-w
9. S.H. Lee, H.L. Park, M.H. Kim, M.H. Kim, B.G. Park, S.D. Lee, Realization of biomimetic synaptic functions in a one-cell organic resistive switching device using the diffusive parameter of conductive filaments. ACS Appl. Mater. Interfaces **12**, 51719–51728 (2020). https://doi.org/10.1021/acsami.0c15519
10. H.L. Park, M.H. Kim, M.H. Kim, S.H. Lee, Reliable organic memristors for neuromorphic computing by predefining a localized ion-migration path in crosslinkable polymer. Nanoscale **12**, 22502–22510 (2020). https://doi.org/10.1039/D0NR06964G
11. S.H. Lee, H.L. Park, M.H. Kim, S. Kang, S.D. Lee, Interfacial triggering of conductive filament growth in organic flexible memristor for high reliability and uniformity. ACS Appl. Mater. Interfaces **11**, 30108–30115 (2019). https://doi.org/10.1021/acsami.9b10491
12. T. Ohno, T. Hasegawa, T. Tsuruoka, K. Terabe, J.K. Gimzewski, M. Aono, Short-term plasticity and long-term potentiation mimicked in single inorganic synapses. Nat. Mater. **10**, 591–595 (2011). https://doi.org/10.1038/nmat3054
13. W. Xu, S.Y. Min, H. Hwang, T.W. Lee, Organic core-sheath nanowire artificial synapses with femtojoule energy consumption. Sci. Adv. **2**, e1501326 (2016). https://doi.org/10.1126/sciadv.1501326
14. Y. Van De Burgt, E. Lubberman, E.J. Fuller, S.T. Keene, G.C. Faria, S. Agarwal et al., A non-volatile organic electrochemical device as a low-voltage artificial synapse for neuromorphic computing. Nat. Mater. **16**, 414–418 (2017). https://doi.org/10.1038/nmat4856
15. Q. Lai, L. Zhang, Z. Li, W.F. Stickle, R.S. Williams, Y. Chen, Ionic/electronic hybrid materials integrated in a synaptic transistor with signal processing and learning functions. Adv. Mater. **22**, 2448–2453 (2010). https://doi.org/10.1002/adma.201000282
16. F. Alibart, S. Pleutin, O. Bichler, C. Gamrat, T. Serrano-Gotarredona, B. Linares-Barranco, D. Vuillaume, A memristive nanoparticle/organic hybrid synapstor for neuroinspired computing. Adv. Func. Mater. **22**, 609–616 (2012). https://doi.org/10.1002/adfm.201101935
17. M. Lee, W. Lee, S. Choi, J.W. Jo, J. Kim, S.K. Park, Y.H. Kim, Brain-inspired photonic neuromorphic devices using photodynamic amorphous oxide semiconductors and their persistent photoconductivity. Adv. Mater. **29**, 1700951 (2017). https://doi.org/10.1002/adma.201700951
18. B. Gholipour, P. Bastock, C. Craig, K. Khan, D. Hewak, C. Soci, Amorphous metal-sulphide microfibers enable photonic synapses for brain-like computing. Adv. Opt. Mater. **3**, 635–641 (2015). https://doi.org/10.1002/adom.201400472
19. H.K. Li, T.P. Chen, P. Liu, S.G. Hu, Y. Liu, Q. Zhang, P.S. Lee, A light-stimulated synaptic transistor with synaptic plasticity and memory functions based on InGaZnOx–Al_2O_3 thin film structure. J. Appl. Phys. **119**, 244505 (2016). https://doi.org/10.1063/1.4955042
20. H.L. Park, J. Jun, M.H. Kim, S.H. Lee, Introduction of helical photonic crystal insulator in organic phototransistor for enhancing

selective color absorption. Org. Electron. **100**, 106385 (2022). https://doi.org/10.1016/j.orgel.2021.106385
21. Y. van De Burgt, A. Melianas, S.T. Keene, G. Malliaras, A. Salleo, Organic electronics for neuromorphic computing. Nat. Electron. **1**, 386–397 (2018). https://doi.org/10.1038/s41928-018-0103-3
22. X. Wu, D. Dai, Y. Ling, S. Chen, C. Huang, S. Feng, W. Huang, Organic single-crystal transistor with unique photo responses and its application as light-stimulated synaptic devices. ACS Appl. Mater. Interfaces **12**, 30627–30634 (2020). https://doi.org/10.1021/acsami.0c05809
23. H.L. Park, S. Kang, J.H. Suh, S.D. Lee, S.H. Lee, Balance of surface energy difference between wetting and dewetting regions for patterning solution-processed organic light-emitting diode. Org. Electron. **95**, 106203 (2021). https://doi.org/10.1016/j.orgel.2021.106203
24. M. Geiger, R. Acharya, E. Reutter, T. Ferschke, U. Zschieschang, J. Weis et al., Effect of the degree of the gate-dielectric surface roughness on the performance of bottom-gate organic thin-film transistors. Adv. Mater. Interfaces **7**, 1902145 (2020). https://doi.org/10.1002/admi.201902145
25. K. Shin, C. Yang, S.Y. Yang, H. Jeon, C.E. Park, Effects of polymer gate dielectrics roughness on pentacene field-effect transistors. Appl. Phys. Lett. **88**, 072109 (2006). https://doi.org/10.1063/1.2176858
26. J. Park, J.S. Choi, Capacitance-voltage characteristics of MIS capacitors using polymeric insulators. J. Inf. Display **9**, 1–4 (2008). https://doi.org/10.1080/15980316.2008.9652049
27. H.L. Park, I.H. Lee, C.M. Keum, S.H. Lee, S.D. Lee, Effect of morphological and physicochemical properties of dielectric-organic semiconductor interfaces on photoresponse of organic phototransistors. Thin Solid Films **619**, 297–301 (2016). https://doi.org/10.1016/j.tsf.2016.10.048
28. S.H. Kim, H. Yang, S.Y. Yang, K. Hong, D. Choi, C. Yang et al., Effect of water in ambient air on hysteresis in pentacene field-effect transistors containing gate dielectrics coated with polymers with different functional groups. Org. Electron. **9**, 673–677 (2008). https://doi.org/10.1016/j.orgel.2008.05.004
29. H. Jiang, Z. Huang, G. Xue, H. Chen, H. Li, Electron transport at the interface of organic semiconductors and hydroxyl-containing dielectrics. J. Mater. Chem. C **6**, 12001–12005 (2018). https://doi.org/10.1039/C8TC01343H
30. J. Kim, S. Cho, Y.H. Kim, S.K. Park, Highly-sensitive solution-processed 2, 8-difluoro-5, 11-bis (triethylsilylethynyl) anthradithiophene (diF-TESADT) phototransistors for optical sensing applications. Org. Electron. **15**, 2099–2106 (2014). https://doi.org/10.1016/j.orgel.2014.06.007
31. W.H. Lee, H.H. Choi, D.H. Kim, K. Cho, 25th anniversary article: microstructure dependent bias stability of organic transistors. Adv. Mater. **26**, 1660–1680 (2014). https://doi.org/10.1002/adma.201304665
32. H. Sirringhaus, Reliability of organic field-effect transistors. Adv. Mater. **21**, 3859–3873 (2009). https://doi.org/10.1002/adma.200901136
33. H.L. Park, Y. Lee, N. Kim, D.G. Seo, G.T. Go, T.W. Lee, Flexible neuromorphic electronics for computing, soft robotics, and neuroprosthetics. Adv. Mater. **32**, 1903558 (2020). https://doi.org/10.1002/adma.201903558
34. D. Choquet, A. Triller, The dynamic synapse. Neuron **80**, 691–703 (2013). https://doi.org/10.1016/j.neuron.2013.10.013
35. J. Yu, X. Yang, G. Gao, Y. Xiong, Y. Wang, J. Han et al., Bioinspired mechano-photonic artificial synapse based on graphene/MoS2 heterostructure. Sci. Adv. **7**, eabd9117 (2021). https://doi.org/10.1126/sciadv.abd9117
36. F. Sun, Q. Lu, S. Feng, T. Zhang, Flexible artificial sensory systems based on neuromorphic devices. ACS Nano **15**, 3875–3899 (2021). https://doi.org/10.1021/acsnano.0c10049
37. J. Gong, H. Wei, Y. Ni, S. Zhang, Y. Du, W. Xu, Methylammonium halide-doped perovskite artificial synapse for light-assisted environmental perception and learning. Mater. Today Phys. **21**, 100540 (2021). https://doi.org/10.1016/j.mtphys.2021.100540